Acta Materialia 126 (2017) 336–345

Contents lists available at ScienceDirect

Acta Materialia

journal homepage: www.elsevier.com/locate/actamat

Full length article

Evolution of superdislocation structures during tertiary creep of a nickel-based single-crystal superalloy at high temperature and low stress

Yuling Tang [a], Ming Huang [a, b], Jichun Xiong [c], Jiarong Li [c], Jing Zhu [a, *]

[a] National Center for Electron Microscopy in Beijing, School of Materials Science and Engineering, The State Key Laboratory of New Ceramics and Fine Processing, Key Laboratory of Advanced Materials (MOE), Tsinghua University, Beijing 100084, People's Republic of China
[b] School of Materials Science and Engineering, Nanjing University of Science and Technology, Nanjing 210094, People's Republic of China
[c] Science and Technology on Advanced High Temperature Structural Materials Laboratory, Beijing Institute of Aeronautical Materials, Beijing 100095, People's Republic of China

ARTICLE INFO

Article history:
Received 31 May 2016
Received in revised form
20 December 2016
Accepted 30 December 2016
Available online 31 December 2016

Keywords:
Nickel-based single-crystal superalloy
Tertiary creep
Electron microscopy
Deformation inhomogeneities
Superdislocations

ABSTRACT

A second-generation nickel-based single crystal superalloys DD6 were creep tested in the [001] direction (within 15°) at 1100 °C/140 MPa. The specimen tested until rupture was investigated using scanning and transmission electron microscopy to determine the evolution of the dislocation behaviors during tertiary creep. It was found that the tertiary creep deformation was highly localized and inhomogeneous along the gauge length, and the types of superdislocations in γ′ rafts varied with the distances from the rupture surface, including individual screw dislocations, antiphase boundary-coupled dislocation pairs, and superlattice intrinsic stacking faults. It can be concluded that γ′ rafts shearing events occur in the following sequence with the evolution of tertiary creep: individual screw dislocations, antiphase boundary-coupled dislocation pairs, and superlattice intrinsic stacking faults. The origin of these transformations of superdislocation types and its influence on tertiary creep rate are discussed. It is proposed that at the microscopic level, a more reasonable explanation for the strain softening mechanism during the tertiary creep of nickel-based superalloys at high temperatures and low stresses is the emergence of new superdislocation types with higher mobility rather than the density rise of a single type of superdislocation produced during the later secondary creep stage.

1. Introduction

Nickel-based single-crystal superalloys have been chosen as materials for high temperature applications such as turbine blades because of their excellent creep properties, corrosion resistance, and fatigue properties [1].

In recent years, with the increasing service temperature of turbine blades, the creep deformation behaviors at temperatures above 1000 °C have attracted much attention [2,3]. One of the most striking issues is links between the dislocation behaviors and creep rate. The interfacial dislocation network formed during the primary creep is relatively stable in the secondary creep stage and could hinder the shearing of γ′ rafts by dislocations from γ channels, thus making a significant contribution to the high temperature creep performance [4–6]. More recently, the coupling of Re, Cr, and Co with interfacial dislocations was suggested to be an additional factor decelerating the secondary creep rate [7]. In the later secondary creep stage, γ′ rafts shearing events were believed to be the dominant recovery process [8–10]. Accordingly, the superdislocation structures were believed to play a crucial role in controlling the secondary creep rate. A new type of a<100> edge superdislocation was frequently reported in this temperature regime [3,11,12]. It was proposed that the movement of a<100> superdislocations relied on a combination of the glide and climb of two $a/2$<110> superpartials with different Burgers vectors [8,13].

In the case of tertiary creep, it is characterized by the progressive strain rate with strain [14–16]. Much modelling work taking into account the creep cavitation and mobile dislocation accumulation has been done to simulate this strain softening phenomenon [14,17–19]. Another important phenomenon at the tertiary creep stage is necking growth that raises the external stress in the

* Corresponding author.
E-mail address: jzhu@mail.tsinghua.edu.cn (J. Zhu).

http://dx.doi.org/10.1016/j.actamat.2016.12.072
1359-6454/

Table 1
Nominal composition of superalloy DD6 (wt.%) [22].

Cr	Co	Mo	W	Ta	Re	Nb	Al	Hf	Ni
4.3	9	2	8	7.5	2	0.5	5.6	0.1	Bal.

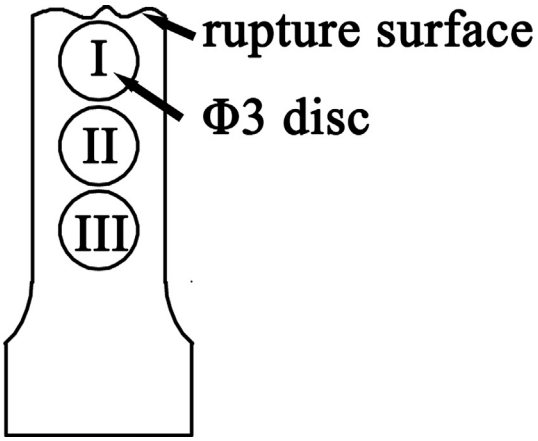

Fig. 1. Schematic of positions of TEM discs taken from specimen B after creep rupture at 1100 °C, 140 MPa. The Φ3 disc I was located just underneath the rupture surface, and discs II and III were located below the disc I, as shown in the figure.

localized region. In addition, the three-dimensional stress state of γ′ rafts could be substantially altered by the load redistribution and local back-up stress accumulation close to the γ/γ′ interface [20]. The stress level and state affect not only the densities but also the types of superdislocations shearing the γ′ rafts. Models focusing on the anisotropic tertiary creep behavior of nickel-based single-crystal superalloys made assumptions that the slip systems {111} <10$\bar{1}$> and {001} <110> were both active [17,21]. Although these models fitted the test data well, it appears that few experimental observations supporting this scenario have yet been reported during tertiary creep at high temperatures. Zhang et al. [3] reported that γ′ rafts in a creep ruptured specimen were sheared by various types of superdislocations, including screw and mixed dislocation pairs, [001] edge dislocations, and superlattice stacking faults. This experimental observation revealed the complex dislocation behaviors during tertiary creep. However, how dislocation activities evolve during tertiary creep and relate to the tertiary creep rate is still not well understood.

Based on the above consideration, the objective of the present work is to capture the evolution of dislocation behaviors that occur during tertiary creep at temperatures above 1000 °C, particularly superdislocations in the γ′ phases and to rationalize their effects on the evolving tertiary creep rate. We investigate the dislocation structures at various distances from the rupture surface, and creep test interrupted at the secondary creep stage was also conducted to clarify the issue better.

2. Experimental

The second-generation nickel-based single-crystal superalloy DD6 was chosen for the present study, and its nominal composition is listed in Table 1 [22]. Creep tests were conducted under a constant load of 140 MPa in the [001] direction at 1100 °C. One specimen was interrupted at 30 h, and is labelled as specimen A. The other specimen, labelled as specimen B, was tested until rupture. Slices were prepared by sectioning from both specimens along a (100) plane, parallel to the applied stress direction. The slices were mechanically polished and etched using a solution consisting of 80 ml H_2O, 100 ml HCl and 20 g $CuSO_4$. The microstructures of these slices were examined using a JEOL 6301F field-emission gun scanning electron microscope (SEM). After the SEM observations, the foils were ground to 50–60 μm. Then, for specimen A, a disc was punched out. For specimen B, three Φ3 discs, labelled as I, II, and III, were punched at different distances from the rupture surface. The Φ3 disc I was located immediately below the rupture surface, and the Φ3 discs II and III were punched below disc I, as illustrated in Fig. 1. Final thinning was performed electrochemically by twin jet polishing with an 8% perchloric acid solution in ethanol at 25 V and −25 °C. The transmission electron microscopy (TEM) studies were conducted using a FEI TECNAI G20 electron microscope. And high angle annular dark field scanning transmission electron microscopy (HADDF STEM) and bright field STEM images were obtained using a probe Cs-corrected JEOL JEM-ARM200F.

3. Results

3.1. γ-γ′ microstructure

The SEM observations of specimen A interrupted at 30 h indicated no significant microstructure changes along the longitudinal direction. The typical microstructure is shown in Fig. 2a. The well-developed γ′ rafting microstructure can be clearly seen in this view. In the case of specimen B, which was tested until rupture, the γ-γ′ microstructure varies with the distance from the rupture surface, as shown in Fig. 2b–d. No obvious creep cavitation was observed along the entire gauge length. At distances of approximately 4 mm and 7 mm away from the rupture surface, the width of the γ channels was basically unchanged compared with the γ channels in specimen A in Fig. 2a. In contrast, the substantial γ channel widening was found at 0.5 mm away from the rupture surface, which was consistent with previous reports [23,24].

3.2. Superdislocation structures

A TEM analysis of the dislocation structures in specimen A and discs I, II, and III taken from specimen B is shown in Fig. 3 where all images were taken close to the zone axis [100]. Morphologically, there are three typical types of superdislocation configurations. The first type of superdislocation, which is indicated by the black arrow, is short and has a zigzag contrast, indicating that it is steeply inclined. The second one, which is marked by the white arrow, is long and contains two parallel partial dislocations. An example of a higher magnification weak-beam dark field image is shown in the inset of Fig. 3c. Another one marked by the white triangle is bounded by the superlattice stacking fault. The γ′ rafts in disc III are sheared by individual dislocations, which are the same as those in specimen A. While those in disc II are additionally sheared by dislocation pairs, and those in disc I are sheared by a large amount of all three types of previously mentioned superdislocations. The nature of these various superdislocation configurations will be carefully analyzed later.

3.2.1. Individual screw dislocations

The nature of the superdislocations marked by the black arrows in Fig. 3 was analyzed using TEM, and the results are summarized in Fig. 4. The Burgers vectors of the dislocations labelled 1 and 2 were analyzed under various two-beam conditions based on the $\boldsymbol{g}\cdot\boldsymbol{b}=0$ or $\boldsymbol{g}\cdot(\boldsymbol{b}\times\boldsymbol{u})=0$ criterion. Dislocation 1 is out of contrast in Fig. 4b for $\boldsymbol{g}=[002]$ and in Fig. 4f for $\boldsymbol{g}=[\bar{1}11]$, while dislocation 2 is out of contrast in Fig. 4a for $\boldsymbol{g}=[0\bar{2}0]$ and in Fig. 4e for $\boldsymbol{g}=[111]$. These observations reveal that the Burgers vectors of dislocations 1 and 2 are parallel to [110] and [10$\bar{1}$], respectively. The magnitude of the